Structural basis for a Kolbe-type decarboxylation catalyzed by a glycyl radical enzyme

Berta M. Martins[†], Martin Blaser[§‡], Mikolaj Feliks[¶], G. Matthias Ullmann[¶], Wolfgang Buckel[§‡] and Thorsten Selmer[§#]*

† Institute für Biologie, Strukturbiologie/Biochemie, Humboldt-Universität zu Berlin, D-10115 Berlin, Germany; §Laboratorium für Mikrobiologie, FB Biologie, Philipps-Universität, D-35032 Marburg, Germany; ‡Max-Planck-Institut für Terrestrische Mikrobiologie, D-35043 Marburg, Germany; ¶Structural Biology/Bioinformatics, Universität Bayreuth, D-95440 Bayreuth, Germany; #AG Biotechnologie/Enzymtechnologie, Fachhochschule Aachen-Jülich, D-52428 Jülich, Germany

Supporting Online Material

References

18. Sebaihia, M.; Wren, B. W.; Mullany, P.; Fairweather, N. F.; Minton, N.; Stabler, R.; Thomson, N. R.; Roberts, A. P.; Cerdeno-Tárraga, A. M.; Wang, H.; Holden, M. T. G.; Wright, A.; Chrucher, C.; Quail, M. A.; Baker, S.; Bason, N.; Brooks, K.; Chillingworth, T.; Cronin, A.; Davis, P.; Dowd, L.; Fraser, A.; Feltwell, T.; Hance, Z.; Holroyd, S.; Jagels, K.; Moule, S.; Mungall, K.; Price, C.; Rabbinowitsch, E.; Sharp, S.; Simmonds, M.; Stevens, K.; Unwin. L.; Whithead, S.; Dupuy, B.; Dougan, G.; Barrel, B.; Parkhill, J. *Nat. Genet.* **2006**, *38*, 779-786.

72. Adams, P. D.; Afonine, P. V.; Bunkoczi, G.; Chen, V. B.; Davis, I. W.; Echols, N.; Headd, J. J.; Hung, L. W.; Kapral, G. J.; Grosse-Kunstleve, R. W.; McCoy, A. J.; Moriarty, N. W.; Oeffner,

R.; Read, R. J.; Richardson, D. C.; Richardson, J. S.; Terwilliger, T. C.; Zwart, P. H. *Acta Crystallogr., Sect. D: Biol. Crystallogr.* **2010**, *66*, 213-221.

79. MacKerell, A. D.; Bashford, D.; Bellott, M.; Dunbrack, R.L.; Jr.; Evanseck, J. D.; Field, M. J.; Fischer, S.; Gao, J.; Guo, H.; Ha, S.; Joseph-McCarthy, D.; Kuchnir, L.; Kuczera, K.; Lau, F. T. K.; Mattos, C.; Michnick, S.; Ngo, T.; Nguyen, D. T.; Prodhom, B.; Reiher, W. E.; Roux, B.; Schlenkrich, M.; Smith, J.C.; Stote, R.; Straub, J.; Watanabe, M.; Wiorkiewicz-Kuczera, J.; Yin, D.; Karplus, M. *J. Phys. Chem. B* **1998**, *102*, 3586-3616.

Table S1. Data collection and refinement statistics

Data set	Substrate-free	Substrate-bound
Total / unique reflections	2,108,535 / 217,979	1,489,089 / 202,600
R_s[a] (%)	9.3 (39.9)	9.9 (33.4)
Resolution (Å)	29.18-1.75	29.16-1.81
Highest resolution shell	1.81-1.75	1.88-1.81
Completeness (%)	97.68 (95.00)	99.82 (99.00)
(I) / (σI)	15.5 (5.7)	13.5 (5.0)
R / R_{free}-factor (%) [b]	18.43 / 22.78	18.81 / 24.42
	(34.15 / 36.76)	(30.39 / 34.74)
Rms deviation from ideal geometry		
Bonds (Å) / Angles (°)	0.007 / 1.085	0.017 / 1.612
ESU[c] (Å)	0.23	0.27
Molprobity output scores (%)		
Rotamers outliers	0.9	2.0
Ramachandran outliers	0.3	0.2
Ramachandran favored	96.7	96.5
Ramachandran allowed	99.7	99.8

Friedel mates were merged for the refinement statistics.

[a] $R_s = \Sigma_h \Sigma_i | I_i(h) - \langle I(h) \rangle | / \Sigma_h \Sigma_i I_i(h)$; where i are the independent observations of reflection h.

[b] The R_{free}-factor was calculated from 5% of the data, which were removed at random before the model was refined.

[c] Estimated overall coordinate error (ESU) based on maximum-likelihood.

Highest-resolution shell values are shown in parentheses.

Table S2. Distances from Cys503Sγ to carboxyl group and to Gly873Cα in the substrate-bound state

Refined values for occupancy and temperature factor (b-factor)	**Cys^{503}Sγ to carboxyl group (distance in Å)**	**Cys^{503}Sγ to Gly^{873}Cα (distance in Å)**
Chain A (occupancy 68% and b-factor 26)	3.3	4.9
Chain A (occupancy 32% and b-factor 18)	4.1	3.9
Chain C (occupancy 57% and b-factor 32)	3.1	4.7
Chain C (occupancy 43% and b-factor 31)	3.6	4.3

Table S3: hydrogen-bonding pattern comparison between γ-subunit and HiPIPs (distances in Å)

N-terminal cluster	C-terminal cluster	1CKU	1ISU
N(ND2)38 – S1 (3.6)	N(N)50 – S2 (3.5)		
C(N)36 – S3 (3.2)		C(N)77 – S3 (3.4)	C(N)55 – S3 (3.4)
H(ND1)3 – S4 (3.1)	R(NH1)61 – S3 (3.4)		
G(O)32 – H3 (2.9)	Water – C(S)45 (3.4)		
S(O)33 – H3 (3.5)			
K(N)40 – C(S)6 (3.6)	N(N)50 – C(S)48 (3.1)	T(N)81 – C(S)46 (3.8)	I(N)59 – C(S)25 (3.5)
K(O)40 – C(S)6 (3.4)			
N(N)38 – C(S)6 (3.3)		F(N)48 – C(S)46 (3.5)	Q(N)27 – C(S)25 (3.4)
L(N)21 – C(S)19 (3.1)	G(N)64 – C(S)62 (3.3)	A(N)65 – C(S)63 (3.3)	V(N)42 – C(S)40 (3.4)
T(N)22 – C(S)19 (3.4)	R(NH2)61 – C(S)62 (3.3)		
N(N)8 – C(S)36 (3.2)	S(N)82 – C(S)80 (3.4)	S(N)79 – C(S)77 (3.4)	A(N)57 – C(S)55 (3.5)
	P(N)81 – C(S)80 (3.3)		

Text S1. The βγ heterodimer and $(\beta\gamma)_4$ heterotetramer interfaces of 4-HPAD$_{Cs}$.

The total buried area in the βγ heterodimer is 3471 Å^2 corresponding to 12% of the heterodimer surface area. The β-subunit contributes to the heterodimer interface with regions Met53-Glu65, Arg167-Lys176 and Asn284-Ile301 from helices surrounding the core barrel and their connecting loops (Ile43-Thr50; Ser84-Tyr93; Lys102-Val104; Met126 and Tyr154-Val157) covering 6% of its molecular surface. The γ-subunit contributes with 30% of its molecular surface including the C-terminal [4Fe-4S] cluster and two of its coordinating cysteines (Cys62 and Cys80). The two stabilizing interfaces within the $(\beta\gamma)_4$ heterotetramer involve the β-subunits. One interface is built by interlocking the helices located at the bottom of the $(\alpha/\beta)_{10}$ core barrel and buries an area of 3729 Å^2. Glycerol dehydratase (PDB ID code 1r9d) and pyruvate formate-lyase (PDB ID code 1h16) display a similar interface for their homodimer arrangement with a more compact interface for pyruvate formate-lyase. The homodimer of pyruvate formate-lyase 2 (PDB ID code 2f3o) is similar but the D2 tetramer is built up by two dimer of dimers rotated by 45°. The homodimer of class III ribonucleotide reductase (PDB ID code 1h7a) is different with the second monomer located at the position of the γ-subunit. The second interface of the $(\beta\gamma)_4$ heterotetramer comprises the helices surrounding the barrel opposite to the βγ heterodimer interface and buries an area of 1739 Å^2. Superposition of all Cα-atoms gives RMS deviation values of 2.1 Å with glycerol dehydratase, 2.5 Å with pyruvate formate-lyase 2, 2.7 Å with pyruvate formate-lyase and 3.3 Å with class III ribonucleotide reductase. The respective sequence identities with 4-HPAD$_{Cs}$ are 28.1, 25.4, 19.7 and 11%.

Supplementary figures and respective captions

Supplementary Figure S1

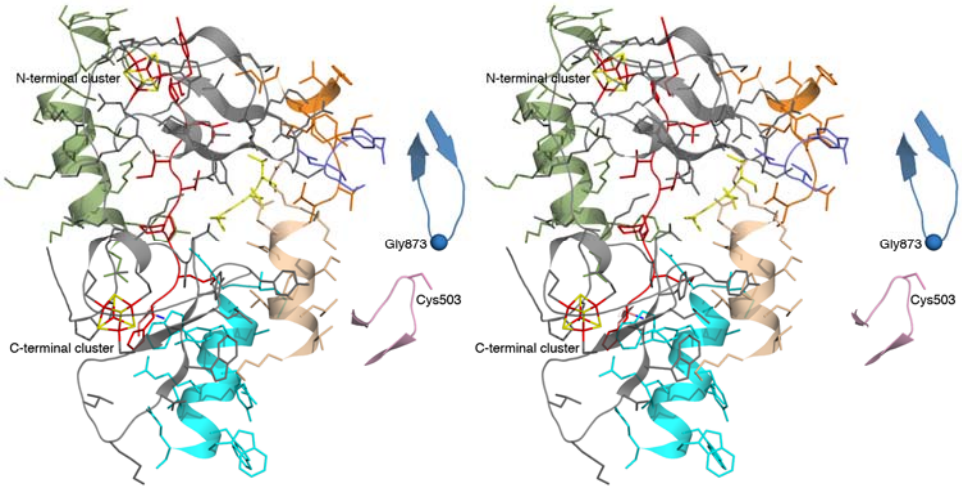

Figure S1. Stereo representation of the βγ heterodimer interface. Residues represented as sticks. The γ-subunit is colored gray with FeS clusters in sticks with red for iron and yellow for sulfur. Coordinating residues are also in sticks. The residues from the β-subunit involved in the interface are Ile43-Thr50 (orange), Met53-Glu65 (cyan), Ser84-Tyr93 (red), Lys102-Val104 (yellow), Tyr154-Val157 (purple), Met167-Lys176 (cream), Asn284-Ile301 (green). Both N- and C-terminal clusters are at 40 Å apart from the active site (Cys503-containing loop in pink and Gly873-containing loop in blue). The inter-cluster distance is 20 Å.

Supplementary Figure S2

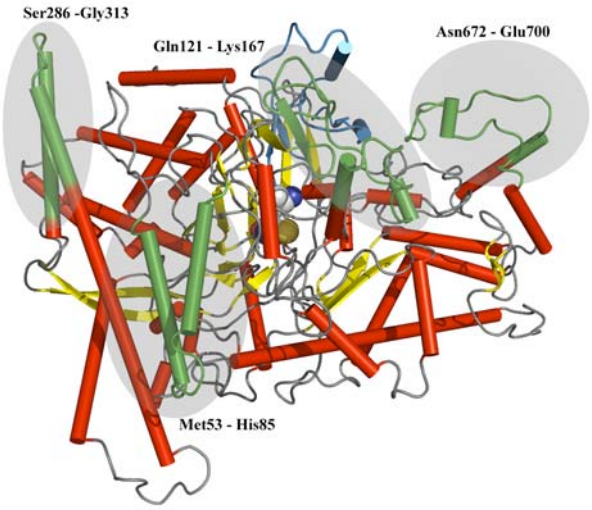

Figure S2. Additional structural features to the canonical GRE. The region Met53-His85 contains a helix-turn-helix motif involved in the $(\beta\gamma)_4$ heterotetramer interface. This topology is conserved in glycerol dehydratase and pyruvate formate-lyase 2, but absent in pyruvate formate-lyase and class III ribonucleotide reductase. The region Ser286-Gly313 (partially present in glycerol dehydratase and pyruvate formate-lyase 2) includes residues from helices involved in the βγ heterodimer interface. The predominantly coil regions Gln121-Lys167 and Asn672-Glu700 located above the barrel is partially present in glycerol dehydratase and pyruvate formate-lyase 2. The radical dyad Cys503/Gly873 is represented as spheres and colored gray for carbon, blue for nitrogen, red for oxygen and yellow for sulfur.

Supplementary Figure S3

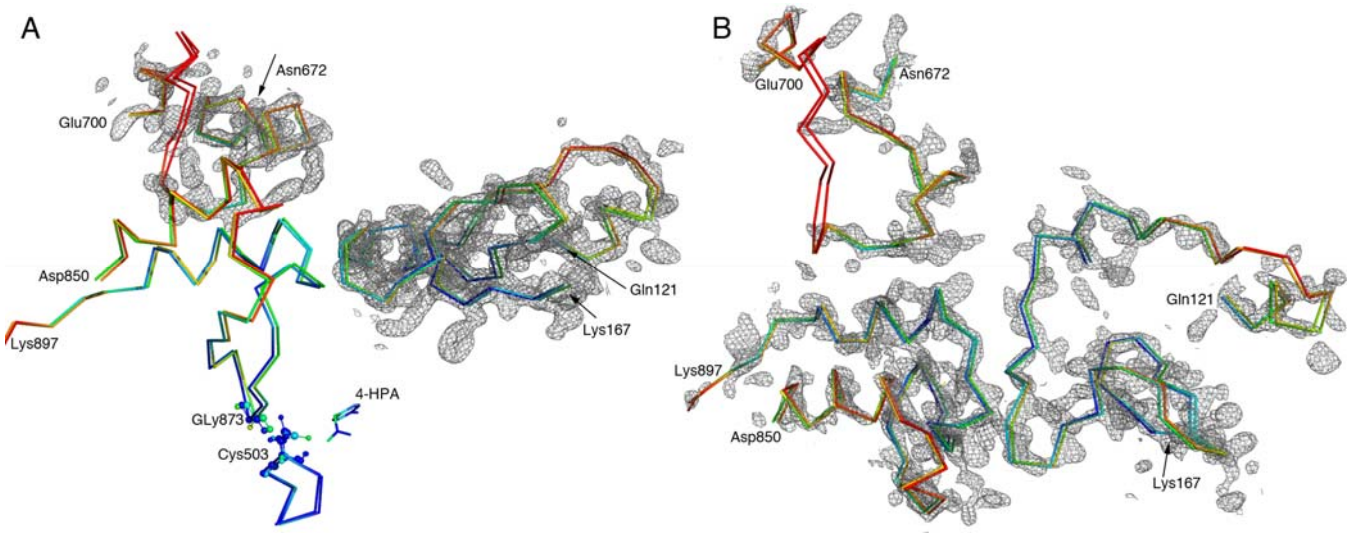

Figure S3. Ribbon representation of the radical domain (Asp850-Lys897) and the peptide regions Gln121-Lys167 and Asn672-Glu700. Color code from blue to red for increasing temperature factor values. The electron density map was contoured at 2.0 sigma. (A) Cys503-containg loop included. The substrate-bound state (by soaking into crystals) shows high temperature factor values as the substrate-free state. The higher temperature factor values are also observed for the Cys503-containg loop of the substrate-bound state. 4-HPA: 4-hydroxyphenylacetate. (B) Up-down rotation view by about 90° to better visualize the weak electron density map for the peptide regions Gly121-Lys167 and Asn672-Glu700 in comparison to the defined electron density map for the radical domain.

Supplementary Figure S4

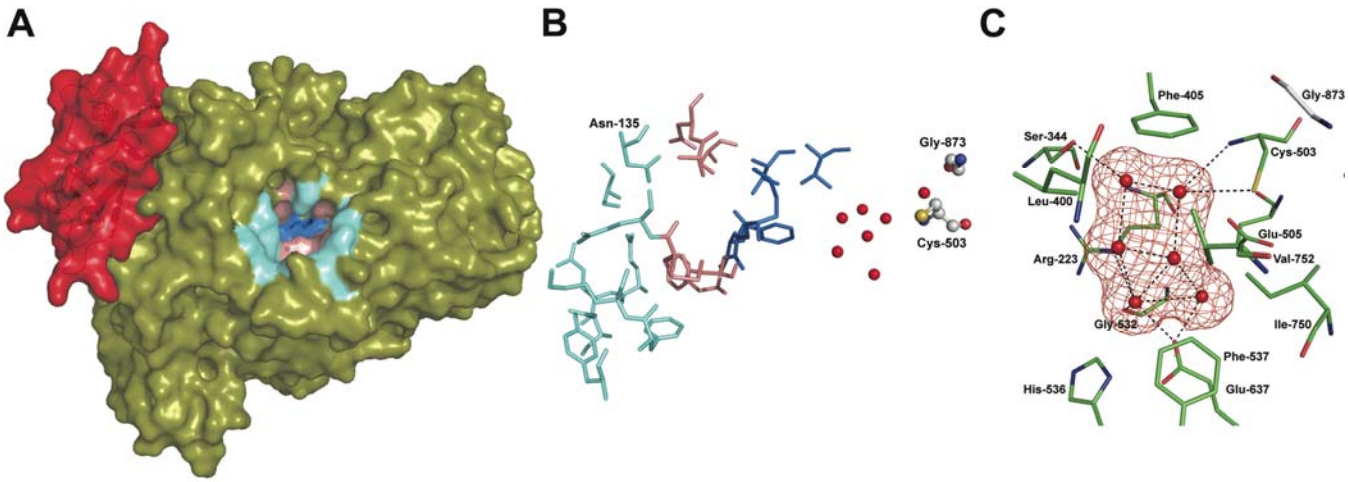

Figure S4. Access to the active site pocket in 4-HPAD$_{Cs}$. (A) Surface representation of the heterodimer with β-subunit in olive and γ-subunit in red. The residues delineating the crevice are divided into three rings for easier visualization. The first ring (cyan) contains Ser116, Asn135, Glu208, Tyr200, Phe203, Glu188, Glu187, Lys204 and Asn191. The second ring (salmon) builds the walls of the crevice and contains Ala137, Asp138, Met207, Asp215, Phe217 and Ser392. The third ring (blue) contains the residues at the entrance of the active site pocket Met213, Phe214, Ala218, Val399 and Val395. (B) The β-subunit was rotated by 90° to the left. Residues color according to ring of origin. Solvent molecules filling the void-volume of the active site are shown as red spheres. Cys503 and Gly873 are colored gray for carbon, blue for nitrogen, blue for oxygen and yellow for sulfur. (C) Active site cavity (red mesh) with residues in sticks and solvent in spheres. Dash lines indicate interactions at hydrogen bonding distances (3.4 Å distance cutoff).

Supplementary Figure S5

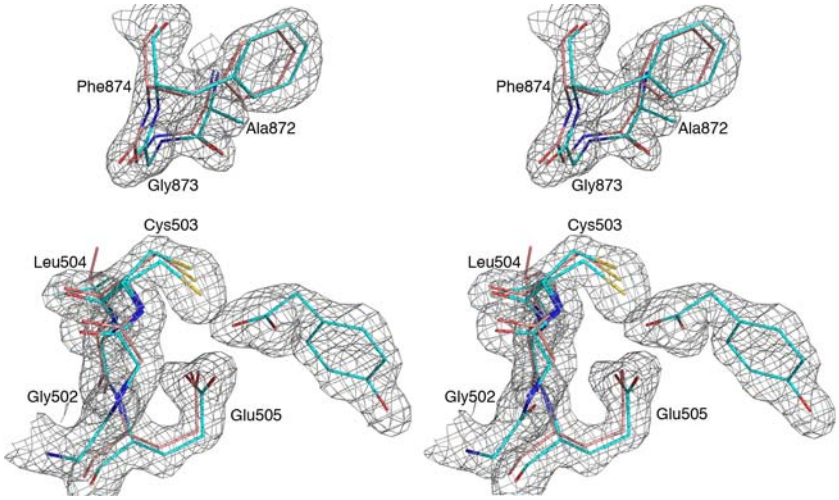

Figure S5. Movement of the Gly873-containing loop towards Cys503-containing loop upon substrate binding. Stick representation of the Cys503- and Gly873-containing loops of substrate-free state (cream) and substrate-bound state (cyan). The electron density map for the substrate bound state was contour at 1.5 sigma. The substrate-bound state was obtained by soaking 4-hydroxyphenylacetate into the crystals, which could preclude major conformational changes that might occur in solution.

Supplementary Figure S6

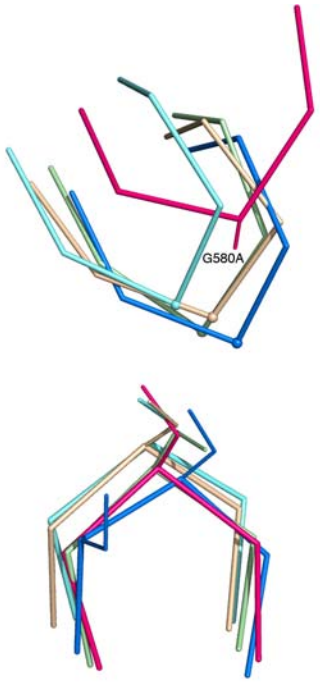

Figure S6: Distance between Cys- and Gly-containing loops in structurally characterized GREs. Ribbon representation of the loops from pyruvate formate-lyase (blue; PDB ID code 1h16), pyruvate formate-lyase 2 (cream; PDB ID code 2f3o), glycerol dehydratase (cyan; PDB ID code 1r9d), class III ribonucleotide reductase (pink; Gly580 was mutated to Ala; PDB ID code 1hk8) and 4-hydroxyphenylacetate decarboxylase (green). The class III ribonucleotide reductase does not overlay well with the GREs. A possible explanation may be because the alanine variant constrains the configurations of the backbone atoms of the Gly-containing loop.

Supplementary Figure S7

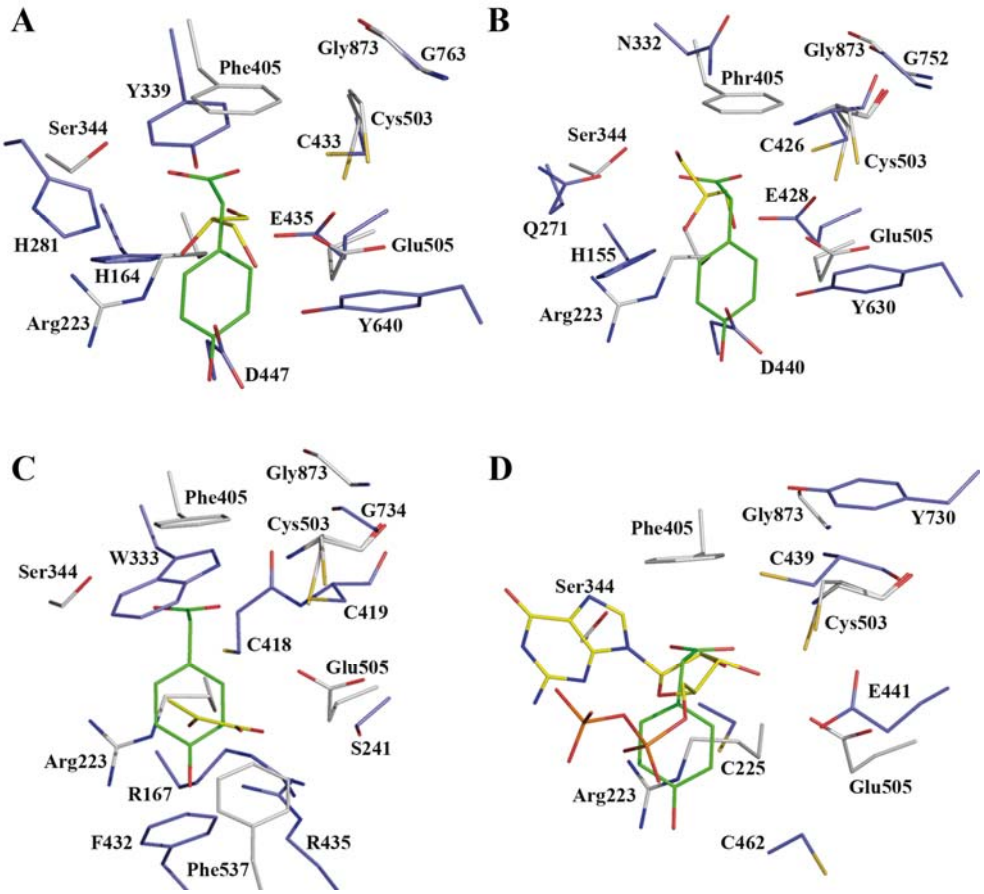

Figure S7. Comparison of active sites and substrate-binding modes in GREs. Residues color is blue for nitrogen, red for oxygen and yellow for sulfur. Carbon color is gray (4-HPAD$_{Cs}$) and violet (other proteins). Substrates are colored yellow for carbon (green for 4-hydroxyphenylacetate), blue for nitrogen, red for oxygen and orange for phosphor. Residue labels are 3 letter-code for 4-HPAD$_{Cs}$ and 1 letter code for other proteins. (A) Superposition with glycerol dehydratase (PDB ID code 1r9d). The active site volume of glycerol dehydratase is reduced due to the side chains of Asp447 and Tyr640. The carboxyl group of 4-hydroxyphenylacetate superimposes with the C2-C3(OH) moiety of glycerol. (B) Superposition with pyruvate formate-lyase 2 (PDB ID code 2f3o). Met632 (omitted for easier view), Asp440 and Tyr630 reduce the active site volume. The carboxyl group of 4-hydroxyphenylacetate superimposes with the C1-C2(OH) moiety of glycerol. (C) Superposition with pyruvate formate-lyase

(PDB ID code 1h16). Arg^{223} (from 4-$HPAD_{Cs}$) is conserved with Arg^{176} that anchors the carboxyl and hydroxyl groups of pyruvate. Phe432 and Trp333 contribute to a reduced volume of the active site. The carboxyl group of 4-hydroxyphenylacetate superimposes with Cys418. (D) Superposition with class I ribonucleotide reductase protein R1 (PDB ID code 4rlr). The acetate moiety of 4-hydroxyphenylacetate superimposes with the ribose ring of guanosine diphosphate with one carboxyl oxygen occupying similar position as the C2'-OH group of guanosine diphosphate. There is no structural information on substrate binding mode for class III ribonucleotide reductase.

Supplementary Figure S8

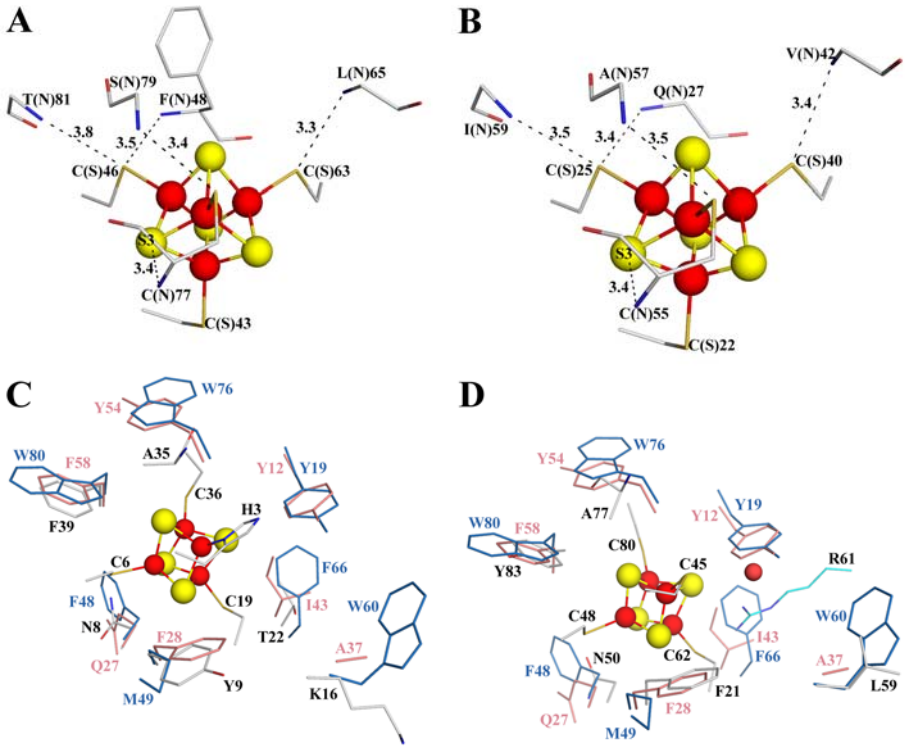

Figure S8: Conserved hydrogen-bonding pattern in HiPIPS and comparison of Fe-S cluster environments with the N- and C-terminal clusters of γ-subunit. (A) Hydrogen bonding pattern in 1cku. (B) Hydrogen bonding pattern in 1isu. Clusters are orientated in similar manner to the N-terminal cluster of γ-subunit (Figure 2C and 2D in manuscript). (C) Comparison of aromatic residues surrounding the N-terminal cluster of γ-subunit and HiPIPS. Color code is blue for 1cku, pink for 1isu and color element for N-terminal cluster of γ-subunit. Tyrosine-19 of 1cku and Tyr12 of 1isu are part of the N-terminal extension present in HiPIPs. (D) Comparison of aromatic residues surrounding the C-terminal cluster of γ-subunit and HiPIPS. Same color code as in (C). Arginine-61 from the β-subunit co-locates with Phe66 from 1cku and Ile43 from 1isu. The water molecule at hydrogen bonding distance from Cys(S)45 is buried in the βγ heterodimer interface. Spatially, it co-locates with Tyr19 and Tyr12 from HiPIPS.

Supplementary Figure S9

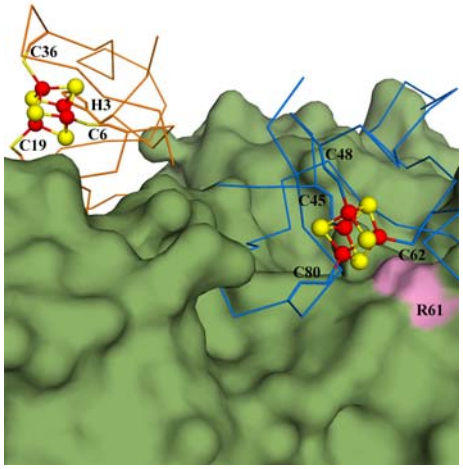

Figure S9: Surface representation of interface between the γ-subunit and the β-subunit. Color code: Orange for N-terminal domain (ribbon representation with Fe-S cluster in red spheres for Fe and yellow spheres for S), blue for C-terminal domain (same representation as N-terminal domain) and green for β-subunit (surface representation). The pink patch indicates the location of Arg61 that is at hydrogen bonding distance to Cys62 from the C-terminal cluster. Cysteine-62 and Cys80 contribute to the βγ heterodimer interface (50 and 60% of respective buried surface are involved in interface) and Cys45 is partially involved (30% of its buried surface). Neither the N-terminal cluster nor its coordinating residues (His3, Cys6, Cys19 and Cys36) are involved in the βγ heterodimer interface.